Modeling of liftoff heights of non-premixed turbulent flames in co-flows having various temperatures and O_2 concentrations

Yuzuru Nada*, Yoshiyuki Kidoguchi, Hidenari Sakai, and Yuto Moriyama

Department of Mechanical Science, Tokushima University, 2-1 Minami-Josanjima, Tokushima 770-8506, Japan

*Corresponding author:
Yuzuru Nada
Department of Mechanical Science, Tokushima University, 2-1 Minami-Josanjima, Tokushima 770-8506, Japan
E-mail address: ynada@tokushima-u.ac.jp
Fax: +81886569124

Declarations of interest: none

Abstract

Lifted flames in combustion furnaces are diluted with burned gas entrained into the fuel jet. The reduced concentrations of reactants resulting from this dilution increase the liftoff height, while the associated temperature increase decreases the height. The aim of the present study was to develop a premixed model capable of predicting the variation in the liftoff height resulting from entrainment. A triple concentric burner incorporating fuel gas, oxidizer and co-flow gas nozzles was employed to simulate a combustion furnace. Prior to combustion tests, the fraction of the fuel gas in the non-reactive jets forming on the burner was determined, to allow an evaluation of parameters affecting the entrainment rate of the co-flow gas. The flame liftoff height above the burner was found to increase with decreases in the O_2 concentration in the co-flow gas and was decreased with increases in temperature. Three premixed models were examined: a conventional premixed model, a DP1 model including only the effect of decreasing reactant concentrations and a DP2 model including the effects of both decreasing concentrations and temperature increases. Validations of these models demonstrated that the conventional model failed to predict variations in the liftoff height at a variety of co-flow gas O_2 concentrations and temperatures. The DP1 model also provided insufficient correlations between the bulk velocity and liftoff height, such that the correlation line at a high co-flow gas temperature separated from that at room temperature. In contrast, the DP2 model provided excellent correlations in conjunction with different virtual origin positions.

Keywords: Turbulent lifted flame, Liftoff height, Premixed model, Dilution, Entrainment

Nomenclature

A : parameter used in Eq. (17) describing the decay of the fuel gas proportion

B : parameter used in Eq. (18) describing the evolution of the jet half width

C_1 : parameter used in Eq. (2) describing the mass flow rate of the entrained co-flow gas

d : inner diameter of the nozzle

$d_{F,ef}$: effective diameter of the nozzle

H : liftoff height

h : enthalpy

K : dilution ratio

L_F : jet half-width based on the fuel gas fraction

M : mass flow rate

m_i : mass of gas i in a fluid

n : the density ratio exponent

r : radial coordinate

S_L: laminar burning velocity

T: temperature

U : bulk velocity at the nozzle exit

X_i : volume fraction of species i

x : axial coordinate

Y_i : mass fraction of species i

Z_i : mixture fraction of gas i

α_C : parameter derived from A

β_C : parameter derived from B

κ : density ratio between the fuel gas and ambient gas

ν : viscosity

ξ : axial distance from the virtual origin

ξ_0 : position of the virtual origin

Subscripts

0 : jet axis

C : co-flow

EN : entrained co-flow gas

F : fuel gas

K : dilution

O : oxidizer

st : stoichiometric condition

1. Introduction

The stabilization of lifted turbulent non-premixed flames is an important aspect of reducing the explosion risks resulting from the accumulation of combustible mixtures in furnaces following flame blow-out and blow-off. In addition, stabilized lifted flames can reduce NOx emissions from furnaces by diluting the combustion mixture with CO_2 and H_2O [1]. Therefore, many researchers have investigated the flame lifting [2,3], stabilization and blow-out [4-11] mechanisms. Lifted flames can be classified as either ignited or non-ignited. In the case that the temperature of the upstream unburned mixture is extremely high, auto-ignition will produce an ignited lifted flame [12]. The key parameter determining the liftoff height in such scenarios is the ignition delay time of the combustible mixture, which can be used to predict the height under high temperature conditions [13, 14]. When the temperature

of the mixture is lower than the auto-ignition point, a non-ignited lifted flame forms. Various theories regarding the stabilization of non-ignited lifted flames have been proposed over the past half a century. Peters and Williams [15] attempted to explain the stabilization mechanism in terms of flame extinction based on a laminar flamelet concept. In their theory, flame extinction occurs in the region between the nozzle exit and the base of the lifted flame because of the higher scalar dissipation rate in this zone. Vanquickenborne and van Tiggelen [16] suggested that lifted flames are stabilized at points at which the gas flow velocity in front of the flame base matches the turbulent burning velocity of a stoichiometric mixture. On this basis, Kalghatgi [17] developed a premixed model to predict the liftoff height from the bulk velocity of the main fuel jet and the laminar burning velocity of the stoichiometric mixture. In contrast, Miake-Lye and Hammer [18] proposed the hypothesis that the base of the lifted flame can propagate upstream in a large-scale structure until the strain rate exceeds a critical value. This model, known as the large eddy model, expresses the liftoff height as a function of the critical strain rate, which in turn is obtained from the laminar burning velocity and thermal diffusivity. Whereas each of the above three theories are based on the assumption that the flame base is fully developed and turbulent, Upatnieks [19] has suggested a model in which different structures appear in the flame base. Upatnieks' group has demonstrated the formation of an edge-flame structure at the base of the turbulent lifted flame using particle image velocimetry (PIV) analyses and also proposed an edge-flame model. In this model, the laminar burning velocity at the flame base is assumed to equal the gas velocity produced by deceleration caused by the gas expansion resulting from heat release [20].

Recently, various groups [4-11] have experimentally investigated the local structures of flame bases appearing in lifted flames using laser diagnostics. Such research established that the stabilization mechanism is associated with the balance between the gas velocity in front of the flame base and the flame propagation speed. However, the structure of the flame base

is also affected by the distance from the nozzle issuing the fuel gas. If a lifted flame forms in a field far from the nozzle, a turbulent premixed flame appears at the flame base [4-7]. In this case, the lifted flame is stabilized owing to the balance between the gas velocity and the turbulent burning velocity [7, 8]. In contrast, the base of a lifted flame that appears in the near field will exhibit an edge-flame structure including a triple flame [9, 10]. As a consequence of the reduced gas velocity that results from the expansion effect near the leading edge, the edge-flame can be stabilized in a gas flow having a high velocity that is greater than the laminar burning velocity [11]. Guiberiti et al. [6] induced a transition from edge-flame to turbulent premixed flame by changing the co-flow velocity and examined this behavior. When the gas velocity near the flame base was less than approximately three times the laminar burning velocity, the edge-flame was stabilized owing to the expansion effect. Otherwise, the flame moved downstream and the base width simultaneously increased because of the decreased gradient of the mixture fraction resulting from the evolution of a mixing layer. Consequently, a turbulent premixed flame formed at the point at which the turbulent burning velocity equaled the gas flow velocity.

The premixed model [17] can adequately predict the liftoff height in the far field, and the edge-flame model [19] could do the same in the near field. In both models, the expressions for the liftoff height are identical except for the exponent applied to the density ratio. The premixed model is more widely used to predict liftoff height [21-24]. Kim et al. [21] demonstrated linear correlations between non-dimensional liftoff heights and bulk jet velocities determined using the premixed model, while Wu et al. [22] applied the model to the study of lifted flames fueled with hydrogen and hydrocarbon mixtures. Min and Baillot [23] modified the premixed model to obtain a correlation for flames in the case that the oxidizer was highly diluted with inert gas. Wang et al. [24] also added a term to the premixed model for the purpose of scaling the liftoff heights at sub-atmospheric pressures.

It should be noted that the scenarios assessed in almost all previous studies were limited to those in which the fuel and oxidizer were mixed with one another. However, in an actual combustion furnace, combustible mixtures of fuel and oxidizer are diluted by the entrainment of hot burned gas that is present throughout the furnace. The extent of dilution of the mixture near the flame base increases along with the liftoff height because the amount of entrained burned gas is proportional to the distance from the nozzle exit to the flame base. Interestingly, dilution with burned gas has two opposite effects on liftoff height. Specifically, the concentrations of reactants in the mixture are reduced while the temperature of the mixture is increased. The former increases the liftoff height while the latter decreases the height, as a consequence of variations in the laminar burning velocity [21] and the magnitude of gas expansion [25]. These opposing effects are intensified as the liftoff height is increased.

In a previous study [26], we examined the effects of decreases in the concentrations of reactants resulting from the entrainment of burned gas. The conditions in an actual combustion furnace were simulated using a triple concentric burner that issued fuel, oxidizer and co-flow gas in conjunction with a lower oxygen concentration while assessing the liftoff height. It is important to note that all gases in this prior work, including the co-flow gas, were at room temperature. This previous research demonstrated that the liftoff height gradually deviated from the heights obtained without co-flow gas dilution as the liftoff height was increased. In addition, we modified both the premixed and large eddy models so as to include the effect of decreasing reactant concentrations on liftoff height.

Although our model provides a suitable correlation between liftoff height and bulk fuel velocity, the effect of temperature increases resulting from the entrainment of hot burned gas is not presently included. The aim of the present work was therefore to model the effect of this factor on the liftoff height. Herein, we firstly explain our modifications to the model, which are intended to reproduce variations in the flame liftoff height associated with co-flow

gases having various reactant concentrations and temperatures. This paper also describes a triple concentric burner allowing the formation of a lifted flame in conjunction with ambient hot co-flow gas, and presents data obtained from assessments of non-reacting jets. These data were used to validate and retrofit our model based on the results obtained from combustion tests. As described herein, the co-flow gas temperatures during our experimental trials were below the values required for immediate ignition, and so the modeling of auto-ignited lifted flames is outside the scope of the present study. However, the present approach to evaluating the effects of burned gas dilution could possibly be used to estimate the ignition delay time in the case that an auto-ignited lifted flame is generated.

2. Modified premixed model

Here, we described the modified premixed model designed to predict variations in the liftoff height with decreases in the concentrations of reactants and temperature increases resulting from entrainment effects. Figure 1 presents a diagram of the generic lifted flame on which the present study was focused. In this scenario, a fuel gas jet and a concentric oxidizer stream are surrounded by a co-flow gas to simulate the burned gas in an actual combustion furnace. The main fuel gas jet entrains the oxidizer and the surrounding co-flow gas, resulting in the formation of a combustible mixture diluted with co-flow gas in front of the flame base. As a consequence of this design, the degree of dilution increases along with the liftoff height. In a previous study [26], we proposed a modified premixed model including the effect of decreasing reactant concentrations on the liftoff flame, referred to as the DP1 model (Diluted and Premixed model version 1) in this article. The model including the temperature rise effect proposed in the present study is termed the DP2 model.

2.1 DP1 model

In the conventional premixed model [17], the non-dimensional liftoff height is proportional to the non-dimensional fuel gas velocity, according to the relationship

$$\frac{S_L H}{\nu_F} \propto \kappa^n \frac{U_F}{S_L}, \tag{1}$$

where S_L is the laminar burning velocity, H is the liftoff height, ν_F is the viscosity of the fuel gas, κ is the ratio of the fuel gas density to that of the ambient gas, n is the exponent applied to this ratio, and U_F is the bulk velocity of the fuel gas at the exit of the main jet nozzle.

In our models, the laminar burning velocity appearing in Eq. (1) is assumed to vary with the extent of dilution, which in turn is determined from the mass flow rate of the co-flow gas entrained up to the point where the fuel gas reaches the base of the lifted flame. On the basis of the mass balance between the three fluids derived from an analysis based on the classical jet theory [27], the mass flow rate of the entrained co-flow gas (M_{EN}) can be obtained as

$$M_{EN} = \frac{32}{C_1}\left(\frac{\xi}{d_{F,ef}}\right) M_F - M_F. \tag{2}$$

Here, ξ is the axial distance from the virtual origin and $d_{F,ef}$ is the effective diameter of the fuel gas nozzle, defined as

$$d_{F,ef} = \left(\frac{\rho_F}{\rho_E}\right) d_F, \tag{3}$$

where ρ_F and ρ_E are the densities of the fuel and reference gases, respectively, and d_F is the diameter of the fuel gas nozzle [28, 29]. M_F is the mass flow rate of the fuel gas issued from the fuel nozzle, and C_1 is a parameter related to the development of the fuel gas jet that was determined from velocity distribution data in a previous study [26]. Using this previously acquired C_1 value and substituting H for ξ in Eq. (2), we can obtain the mass flow rate of the co-flow gas entrained into the mixture in the vicinity of the flame base.

The entrained co-flow gas is assumed to preferentially mix with the oxidizer rather than the fuel gas. This effect is referred to as oxidizer-side dilution [23, 30] and the oxidizer dilution ratio (K_O) is defined as

$$K_O = \frac{M_{EN}}{M_O + M_{EN}}, \tag{4}$$

where M_O is the mass flow rate of the oxidizer. The mass fraction of each species in the oxidizer diluted with the co-flow gas ($Y_{i,O,K}$) can then be calculated using the oxidizer dilution ratio as

$$Y_{i,O,K} = (1 - K_O)Y_{i,O} + K_O Y_{i,C}, \tag{5}$$

where $Y_{i,O}$ and $Y_{i,C}$ are the initial mass fractions of species i in the oxidizer and co-flow gas, respectively. The diluted oxidizer and fuel gas combine to generate a stoichiometric mixture in which the mass fraction of species i ($Y_{i,K,st}$) is

$$Y_{i,K,st} = (1 - Z_{st})Y_{i,O,K} + Z_{st}Y_{i,F}. \tag{6}$$

Here, $Y_{i,F}$ is the mass fraction of the species in the fuel gas at the fuel nozzle exit and Z_{st} is the stoichiometric mixture fraction determined based on $Y_{i,O,K}$ and $Y_{i,F}$. Since premixed flames existing at the flame base are assumed to propagate in the stoichiometric mixture, the laminar burning velocity can be determined from the properties of the mixture. Consequently, the DP1 model can be summarized by the equation

$$\frac{S_{L,K}H}{\nu_F} \propto \kappa^n \frac{U_F}{S_{L,K}}, \tag{7}$$

where

$$\kappa = \frac{\rho_F}{\rho_O}. \tag{8}$$

Here, $S_{L,K}$ is the laminar burning velocity for a specific $Y_{i,K,st}$ value and κ is the ratio between the fuel density, ρ_F, and oxidizer density, ρ_O. The DP1 model was found to provide accurate linear correlations between the bulk velocities and liftoff heights of flames for a range of O_2 concentrations in the co-flow gas [26].

2.2 DP2 model

In the present study, we propose the DP2 model, which includes the effects of the temperature rise resulting from the entrainment of the hot co-flow gas. The mass flow rate of the entrained co-flow gas (M_{EN}) is estimated in the same manner as in the DP1 model. The temperature of the diluted stoichiometric mixture ($T_{K,st}$) is calculated from the enthalpy ($h_{K,st}$), which in turn is obtained from the relationship

$$h_{K,st} = (1 - Z_{st})h_{O,K} + Z_{st}h_F, \quad (9)$$

where h_F is the enthalpy of the fuel gas and $h_{O,K}$ is the enthalpy of the diluted oxidizer. The latter value can be estimated from the relationship

$$h_{O,K} = (1 - K_O)h_O + K_O h_C, \quad (10)$$

in which h_O and h_C are the enthalpies of the oxidizer and co-flow gas, respectively. The temperature of the diluted oxidizer ($T_{O,K}$) can also be obtained using $h_{O,K}$ and $Y_{i,O,K}$.

In this work, the laminar burning velocities at a variety of $T_{K,st}$ and $Y_{i,K,st}$ were calculated using the CHEMKIN II PREMIX program [31] combined with the detailed kinetics mechanism proposed by Qin et al. [32]. This mechanism has been shown to accurately predict the laminar burning velocities of high temperature mixtures diluted with N_2 and CO_2 [33, 34]. Because the mass flow rate of the entrained co-flow gas increases along with the liftoff height, the laminar burning velocity also varies with the height, and the incorporation of this relationship is a feature of our revised model. The DP2 model is therefore expressed as

$$\frac{S_{L,K}H}{\nu_F} \propto {\kappa_K}^n \frac{U_F}{S_{L,K}}, \quad (11)$$

where

$$\kappa_K = \frac{\rho_F}{\rho_{O,K}}. \quad (12)$$

Note that the ratio of the density of the fuel gas to that of the diluted oxidizer (κ_K) is employed in Eq. (11) instead of the κ defined in Eq. (8). In Eq. (12), $\rho_{O,K}$ is the density of the oxidizer diluted with entrained co-flow gas, which is obtained using $Y_{i,O,K}$ and $T_{O,K}$. Accordingly, the density ratio will also vary with the liftoff height. The density ratio is defined as the ratio between the main jet and surrounding gas as in the original paper [17]. Since the base of a lifted flame is surrounded by the oxidizer diluted with the co-flow gas, we believe it is reasonable to use the density of the diluted oxidizer as a representative value rather than that of the pure oxidizer. This modification was not incorporated in our previous study [26] because the experiments were performed at room temperature. However, the effect of increases in the density ratio due to the lower density of the hot co-flow gas is important in the present study.

3. Experimental setup

3.1 Triple concentric burner

Figure 2 provides a diagram of the experimental apparatus and of the triple concentric burner, which comprised fuel gas, oxidizer and co-flow nozzles. The inner diameters of these nozzles were 2, 30 and 172 mm, respectively, while the rim thickness and fuel gas nozzle length were 0.5 and 900 mm. Honeycomb-type materials were installed in the oxidizer and co-flow nozzles to ensure uniform flows and ceramic beads were embedded in the lower section of the co-flow nozzle. The side wall of the co-flow nozzle was heated using an electrical heater to minimize heat loss from the hot co-flow gas to the wall. A glass tube with an inner diameter of 182 mm and a length of 300 mm was mounted on the burner to prevent the hot co-flow gas from mixing with the ambient air. The burner and the glass tube were located in a large housing with a 720 × 720 mm cross-section. In this paper, a cylindrical

coordinate system (x, r) is used to present positions, with the origin of the system located at the center of the fuel nozzle exit and the x-coordinates moving in the positive direction vertically upward.

A mixture of C_3H_8 and a diluent was used as a fuel gas during the combustion tests, with either N_2 or CO_2 serving as the diluent. Whereas the oxidizer was pure air, the co-flow gas was a mixture of air and the same diluent used in the corresponding fuel gas (see Table 1). Air was supplied from a compressor and the other gases were obtained from pressurized bottles. The mass flow rate of each gas was controlled at a designated value by calibrated rotameters and needle valves. These gases were combined with one another after which the resulting mixtures were introduced into the burner. The co-flow gas passed through electrical heaters before entering the burner, such that the co-flow gas temperature at the nozzle exit (T_C) was approximately 640 K when the heaters were operated.

3.2 Experimental conditions during combustion tests

The fuel gas and co-flow gas compositions used in this work are summarized in Table 1. In the case of flames diluted with N_2 (termed LF1 in the table), the fuel gas was a mixture of 70% C_3H_8 and 30% N_2 (all percentages provided herein are on a volume basis), with an uncertainty of 1.3% in the C_3H_8 concentration. Air diluted with N_2 was used as the co-flow gas, with O_2 concentrations ($X_{O2,C}$) from 21% (without a diluent) to 18%, with an uncertainty of 0.06%. In contrast, flames diluted with CO_2 (LF2) were generated using fuel gas comprising 70% C_3H_8 and 30% CO_2 while the co-flow gas was a mixture of air and CO_2 in which the range of $X_{O2,C}$ was from 21% to 19%. The minimum $X_{O2,C}$ value for the LF2 trials was higher than that for the LF1 tests because the laminar flame at $X_{O2,C}$ = 18% was found to blow out prior to transitioning to a turbulent flame. This likely occurred because the H radicals required for a chain reaction were wastefully consumed during decomposition of

CO_2 to CO [35], resulting in a decrease in the laminar burning velocity. The oxidizer was air without pre-dilution during all experimental trials.

During the combustion tests, we employed co-flow gas temperatures, T_C, of 300 and 640 K. During the T_C = 640 K trials, the fuel gas and oxidizer were simultaneously heated by the hot co-flow stream and by the heater mounted external to the co-flow gas nozzle. The resulting temperatures of the fuel gas and oxidizer at the exit of the corresponding nozzles were determined to be 315 and 350 K, respectively. The bulk velocity of the fuel gas was varied from 6 to 23 m/s, with an uncertainty of 0.19 m/s. The maximum velocity was determined by the highest flow rate that could be measured by the rotameter that was used. During the T_C = 300 K tests, the bulk velocities of the oxidizer and co-flow gas were both 0.2 ± 0.003 m/s. In contrast, at T_C = 640 K, the gas streams were accelerated owing to the increased temperature. Because the mass flow rate of each gas was maintained regardless of the co-flow temperature, the resulting velocities of the oxidizer and co-flow gas at T_C = 640 K were estimated to be 0.23 and 0.43 m/s, assuming that the pressure remained constant.

3.3 Measurements

Lifted heights were measured using the same technique employed in our previous study [26]. The flame above the burner was initially lifted by applying a very high fuel gas velocity, after which the velocity was adjusted to a designated value. More than 200 images of lifted flames were captured through a glass window on the lateral side of the housing, using a digital camera (Nikon D90) with a shutter speed of 1/125, *f*-number of 3.5 and ISO speed of 400. The spatial resolution of each image was 0.2 mm/pixel and these images were subsequently binarized using an adequate threshold to identify the leading edge of the lifted flame. The edge positions were averaged to ascertain the mean liftoff height and its fluctuations. Details of this image analysis process have been previously published [26].

As described in the previous section with regard to Eq. (2), our models required the parameter C_1 to estimate the entrainment rate. In the present study, we obtained the value of C_1 from the distribution of the fuel gas fraction (Z_F), defined as

$$Z_F = \frac{m_F}{m_F+m_O+m_{EN}}, \tag{13}$$

where m is the mass of each fluid. The value of this mixture fraction could be calculated from the equations

$$Y_i = Y_{i,F}Z_F + Y_{i,O}Z_O + Y_{i,C}Z_C \tag{14}$$

and

$$Z_F + Z_O + Z_C = 1. \tag{15}$$

Here, Z is the mixture fraction of each fluid, Y_i is the measured mass fraction of species i, and $Y_{i,F}$, $Y_{i,O}$ and $Y_{i,C}$ are the mass fractions of species i in the fuel gas, oxidizer and co-flow gas issued from the nozzles, respectively.

The concentrations of various species were assessed in non-reacting jets for safety reasons, during which we employed the composition as a marker for each flow, as shown in Table 2. The concentration of each species in each flow was determined so that the variations in concentrations between flows was as large as possible within the range of values that could be monitored in our experimental system. In addition, the flow densities were comparable to those obtained in the LF1 trial with $X_{O2,C}$ = 21%, as shown in Table 1. The CO_2 and O_2 concentrations were measured using a gas analyzer (HORIBA PG-250) with an L-shaped sampling probe having an inner diameter of 1.5 mm at a sampling flow rate of 0.5 L/min. Each concentration was recorded in a data logger with a sampling frequency of 1 Hz over a span of 60 s after the measured value became stable. During these trials, the bulk velocity of the main jet was held constant at 21 m/s and the remaining experimental conditions (that is, the flow velocities and temperatures) were the same as those during the combustion tests.

3.4 Uniformity of temperature distribution

The uniformity of the temperature distribution at the exit of the co-flow nozzle was confirmed by measuring the temperature above the burner using a thermocouple while operating the heaters. Temperature data were acquired at a frequency of 10 Hz and were averaged over a span of 150 s. A mixture comprising 70% CO_2 and 30% N_2 was used as the main jet gas (instead of a reactive mixture of C_3H_8 and N_2) at a bulk velocity of 21 m/s, while the compositions and velocities of the other flows were identical to those used in the combustion tests performed with preheating but without pre-dilution of the co-flow gas. Figure 3 presents the radial distributions of temperature at different heights from the nozzle exit. The temperature distributions in the region for which $r \geq 20$ mm, which coincided with the area above the co-flow nozzle, were suitably uniform based on spatial fluctuations of less than 10 K. The spatial average of the temperature in the region of 60 mm $\geq r \geq$ 20 mm was 640 K at x = 10 mm. Hereafter, the representative temperature of the co-flow gas, which is used in the DP2 model, is set to 640 K. The co-flow temperature steeply decreased moving radially toward the jet axis in the region of $r < 20$ mm, because of the effects of the cold fuel jet and oxidizer flow.

4. Results

4.1. Characteristics of non-reactive jets

In this subsection, we describe the characteristics of non-reactive jets related to the determination of C_1, which in turn was used to estimate the mass flow rate of the co-flow gas entrained into the fuel gas jet. C_1 can be expressed as a function of the parameters A and B, which are associated with the decay and spread of the jet, respectively. This relationship is written as [26]

$$C_1 = \frac{16A}{B^2}\ln(2). \quad (16)$$

The inverse of the mixture fraction along the jet axis ($1 / Z_{F,0}$) is known to be directly proportional to the distance from the virtual origin, describing a linear relationship with a slope of $2A$ [28, 29], as in the equation

$$\frac{1}{Z_{F,0}} = 2A\frac{\xi}{d_{F,ef}}. \quad (17)$$

Note that, in the present study, the oxidizer density was employed as the reference density used to calculate the effective diameter, $d_{F,ef}$, via Eq. (3).

The jet half-width (L_F), defined as the radius at which the mixture fraction is half of $Z_{F,0}$, also increases linearly but with a slope of B as [29]

$$L_F = B\xi. \quad (18)$$

The radial profiles of the fuel gas mixture fraction in similarity form are presented in Fig. 4, in which the solid line represents the profile estimated from an empirical formula [28].

$$Z_F/Z_{F,0} = \exp\{-(r/L_F)^2\ln(2)\}. \quad (19)$$

Note also that the mixture fractions and radial coordinate values in this figure have been normalized by $Z_{F,0}$ and L_F, respectively. As shown in Fig. 4(a), the profile for the normalized mixture fraction in the jet formed at T_C = 300 K showed good agreement with that obtained from the empirical formula. The mixture fraction at T_C = 640 K (Fig. 4(b)) also showed acceptable similarities even though the values in the region near the edge of the jet ($1.0 < r/L_F < 2.0$) deviated from the empirical profile. Figure 5(a) summarizes the decay of the fuel gas mixture fraction along the jet axis. The inverse of $Z_{F,0}$ increased linearly with the distance from the fuel nozzle exit regardless of the co-flow temperature, and the plots in both cases coincided with a single line. In contrast, the spread of the jet width exhibited different behavior with respect to the co-flow temperature, as shown in Fig. 5(b). Although the slopes of the jet width in both cases were equivalent, the widths at T_C = 640 K were larger than those at T_C = 300 K. This discrepancy can likely be attributed to the lower density of the high-temperature co-flow gas as compared with the other streams. This lower density would

be expected to induce unstable flow near the nozzle exit and to subsequently enhance mixing among these fluids.

The slopes of the $1/Z_{F,0}$ and L_F data provide other important jet parameters in addition to C_1, which are summarized in Table 3. Lawn [28] published a review in which the parameters α_C (= $1/A$) and β_C (= $\ln(2)/B^2$) from other published papers [36-39] are summarized, from which it is evident that the ranges of reported α_C and β_C values are from 8.9 to 10.1 and from 56 to 67, respectively. Our values for α_C, which were 9.1 at T_C = 300 K and 9.0 at T_C = 640 K, were within the associated range, although the present β_C values (78.9 at T_C = 300 K and 80.4 at T_C = 640 K) were not. As a result, the calculated C_1 values of 138.8 and 143.2 exceeded the value of 103 employed in our previous study [26]. It should be noted that we employed the oxidizer density as the reference density in Eq. (3), whereas the co-flow density was used for this parameter in a previous study [26]. At T_C = 300 K, which was the condition applied in the previous work, the density of the co-flow gas was comparable to that of the oxidizer because both gases were at the same temperature. Consequently, the gas used to provide the reference density did not affect the jet evolution calculations. However, at T_C = 640 K, the co-flow density was much lower than that of the oxidizer, such that the C_1 value was increased to 186 when using the co-flow density. To avoid applying an unrealistic value for C_1, we therefore selected the oxidizer density for use as the reference value in Eq. (3).

In our models, the large width of the jet at T_C = 640 K was represented by movement of the virtual origin. Two different techniques have been suggested for determining the position of the virtual origin, based on the velocity decay along the jet axis [28] or the width of the jet [40]. We employed the latter method, such that the virtual origin was located at the position at which the width of the jet had a value of zero. This position was determined by extrapolation of the approximated line shown in Fig. 5(b), and the resulting virtual origin positions were -2.8 mm at T_C = 300 K and -9.0 mm at T_C = 640 K. In Lawn's review [28], the

positions were reported to be in the range from -3.5 d_F to d_F, which corresponds to -7 mm to 2 mm for our burner. Hence, the position at T_C = 640 K might be excessive, and the validity of this result is discussed in section 5.

4.2. Modeling of liftoff height

Figure 6 shows the variations in the mean liftoff height with respect to the bulk velocity of the fuel gas under various conditions. In these figures, the error bars indicate the standard deviations of the liftoff heights. As demonstrated in our previous study [26], the liftoff height tends to increase with decreasing O_2 concentrations in the co-flow gas regardless of the co-flow temperature or the type of diluent, which indicates the significant impact of dilution with the co-flow gas on the liftoff height. The use of CO_2 as the diluent increased the liftoff height compared with the results obtained using N_2, as a consequence of the chemical effect of CO_2 [34]. Increasing the temperature of the co-flow gas produced lower liftoff heights due to the increases in the laminar burning velocity.

Figure 7(a) presents the liftoff height correlations with the non-dimensional bulk velocity obtained using the conventional premixed model (Eq. (1)), in which the effects of dilution and temperature rise resulting from the entrainment of the co-flow gas are neglected. Here, the laminar burning velocity values were determined from the concentration and temperature of the stoichiometric mixture composed of the fuel gas and non-diluted oxidizer. The density ratios were calculated from the density values for the fuel gas and oxidizer ($\kappa = \rho_F / \rho_O$), applying an exponent of 1.5 according to Kalghatgi's analysis [17]. At $X_{O2,C}$ = 21% and T_C = 300 K, the correlation obtained for the LF1 flames coincided with that for the LF2 flames and the associated slope of 46.6 was comparable to that of 50.1 reported by Kalghatgi (see the solid line in this figure). However, as was also the case in our previous study [26], it is apparent that the conventional model failed to accurately predict the liftoff heights at lower

O_2 concentrations regardless of the co-flow temperature. Although the HS_L/ν_F values of lifted flames exiting at lower heights were comparable, the values of HS_L/ν_F deviated from those at $X_{O2,C}$ = 21% as the liftoff height was increased. This was due to the significant effects of dilution, which were enhanced with increases in the liftoff height. The results acquired at T_C = 640 K are plotted below those at T_C = 300 K and demonstrate that the conventional model under-predicted the laminar burning velocity at T_C = 640 K. This discrepancy is ascribed to the failure of the conventional model to take into account the effect of the temperature rise accompanying dilution with the hot co-flow gas.

The liftoff height correlations obtained from the DP1 model (Eqs. (7) and (8)) are provided in Fig. 7(b). The laminar burning velocity in this model is a function of both $Y_{i,K,st}$ (Eq. (6)) and T_{st}, which is the temperature calculated using Eq. (9) assuming that the co-flow temperature is equal to that of the oxidizer. Therefore, the effect of the increased temperature produced by entrainment of the hot co-flow gas is not included in DP1 model. During this analysis, the exponent applied to the density ratio was maintained at 1.5 and the virtual origin position was assumed to be zero (ξ_0 = 0). Since the DP1 model was able to reproduce variations in the liftoff height resulting from decreases in the reactant concentration, an excellent correlation was obtained at each co-flow temperature. The slope of the correlation at T_C = 300 K was 48.7, which is similar to Kalghatgi's slope. In contrast, the slope at T_C = 640 K had a lower value of 9.4, indicating that the DP1 model also under-predicted the laminar burning velocity when the co-flow temperature was higher than those of the other streams.

Figure 8 shows the liftoff height correlation obtained from the DP2 model, in which both the effects of the decreasing reactant concentrations and increasing temperature are included. Figure 8(a) presents the results for an n value of 1.5 in Eq. (11), while Fig. 8(b) shows the data for n = 1.0. A comparison of these data with those in Figs. 7(b) and 8(a)

indicates that the introduction of the temperature rise effect into our model increased the slope of the correlation at T_C = 640 K while the slope at T_C = 300 K was maintained. However, the large difference between the correlation lines at T_C = 300 K and T_C = 640 K remained. Therefore, we adjusted the density ratio exponent from 1.5 to 1.0 (see Fig. 8(b)). This adjustment caused the correlation at T_C = 640 K to approach that at T_C = 300 K even though the slope of the correlation at T_C = 300 K also increased from 48.7 to 57.5. In addition, the plots at T_C = 300 K for n = 1.0 were more widely distributed than those for n = 1.5.

Finally, we introduced the effect of the virtual origin into our model so as to match the correlations at T_C = 640 K to those at T_C = 300 K. The liftoff height was re-defined as the distance from the virtual origin to the flame base (= H - ξ_0), according to the relationship

$$\frac{S_{L,K}(H-\xi_0)}{\nu_F} \propto \kappa_K \frac{U_F}{S_{L,K}}. \quad (20)$$

In addition, the mass flow rate of the entrained co-flow gas was evaluated based on this distance, using the relationship

$$M_{EN} = \frac{32}{C_1}\left(\frac{H-\xi_0}{d_{F,ef}}\right) M_F - M_F. \quad (21)$$

In prior work [17, 18], variations in the virtual origin were ignored. However, because the original models were based on jet similarity theory, the liftoff height could also be defined as the distance from the virtual origin. As shown in Fig. 9, we were able to obtain linear correlations for the results obtained under all conditions using the DP2 model when including the virtual origin effect. In addition, the correlation slope of 52.9 was comparable to that of 46.6 reported by Wu et al. [22]. The results presented in Figs. 8 and 9 confirm the importance of considering the jet characteristics associated with the virtual origin as well as the extent of entrainment when predicting the liftoff heights of flames in conjunction with hot co-flow gas.

5. Discussion

As shown in Fig. 9, we successfully scaled the liftoff heights using the DP2 model, for which the modifications from the DP1 model can be summarized as:

M1, related to increases in the laminar burning velocity due to the temperature rise,

M2, related to the density of the diluted oxidizer,

M3, related to changing the exponent applied to the density ratio from 1.5 to 1.0, and

M4, related to the introduction of the virtual origin.

M1 and M2 are fundamental to the DP2 model. The former enables the laminar burning velocity to increase along with the mass flow rate of the entrained hot co-flow gas, resulting in an increased slope for the correlation between $\kappa_K U_F$ / $S_{L,K}$ and $HS_{L,K}$ / ν_F. In contrast, M2 moderates the increase in the slope resulting from M1. At higher co-flow temperatures, the value of κ_K (= ρ_F / $\rho_{O,K}$) increased along with the liftoff height because of the decreasing density of the oxidizer ($\rho_{O,K}$) associated with dilution due to the entrainment of hot gas. Accordingly, the value of the non-dimensional velocity (= $\kappa_K U_F$ / $S_{L,K}$) was also increased, lowering the slope of the correlation.

The selection of the representative density appearing in the density ratio of the premixed model was discussed by Min and Baillot [23], who eventually employed the density of pure air in order to obtain a linear correlation, even though the air used was diluted with inert gas. However, as pointed out by Min and Baillot [23], this represents a compromise, and hence the densities used in the premixed model should preferably be those of the gases actually used during the experimental trials. Therefore, we employed the density of the diluted oxidizer in the DP2 model. The use of 1.0 as the exponent for the density ratio (M3) is considered to be an acceptable modification. Originally, the density ratio was added to the model simply so that the liftoff heights of flames fueled with different gases merged on a

single line [17]. As an example, Wu et al. [22] employed a value of 1.0 for the exponent to obtain a linear correlation for flames fueled with H_2 diluted with CO_2 and C_3H_8.

The introduction of the virtual origin (M4) could be considered somewhat arbitrary, even though the DP2 model including the virtual origin effect exhibits a satisfactory correlation in Fig. 9. In the present work, we evaluated the position of the origin based on the jet width, as explained in the previous section. An evaluation using a different process based on the variation in the mixture fraction along the jet axis [28] gave a different trend such that the positions at T_C = 640 K and T_C = 300 K were both 0.5 mm. In addition, the virtual origin obtained at T_C = 640 K was over the upper limit provided in Lawn's review [28]. Nevertheless, we employed the position based on the jet width because the hot co-flow stream generated intense mixing of the surrounding gas, which would be expected to promote the evolution of the fuel gas jet. This mixing in turn reduced the length of the potential core in the main jet, as reflected in the movement of the virtual origin upstream in the case of the DP2 model. Unfortunately, we did not obtain direct evidence for enhanced mixing at the boundary of the fuel gas jet because the inherent mixing of the jet obscured any additional mixing. However, we did observe intense mixing between the hot co-flow gas and ambient air in the housing when the glass tube on the burner was dismounted. The effect of this mixing extended to the vicinity of the oxidizer nozzle, and hence the temperature distribution external to the concentric nozzle was significantly disturbed. This finding indicates that the intense mixing induced by the hot co-flow gas increased the entrainment of the oxidizer and co-flow gas into the fuel gas jet.

The above hypothesis is reinforced by the negative buoyancy effect proposed by Van et al. [41-43]. In these prior reports, the effect of buoyancy on the behavior of a lifted laminar flame was broken down into two phenomena (see Figure 8 in ref. [41]). The positive effect was based on the buoyancy force induced by the density difference between unburned and

burned gases, and tended to increase the liftoff height as the fuel velocity decreased [42]. In contrast, the negative effect was based on the difference between the fuel gas and co-flow densities, and provided an oscillating lifted flame [43]. In the present study, the fuel gas velocity was much higher than that employed in the work of Van et al., and hence the buoyancy forces directly acting on the main fuel jet could be neglected. Therefore, the positive buoyancy effect, which pulls up the lifted flame, was also negligible. Even so, because the oxidizer stream was much slower than the main fuel jet, there was likely a buoyancy effect acting on the oxidizer gas. In addition, the oxidizer gas was heavier than the co-flow gas, which was located external to the oxidizer gas flow, at T_C = 640 K. Consequently, there was a negative buoyancy acting on the oxidizer stream, forming recirculation vortices in the vicinity of the oxidizer nozzle exit. These vortices would be expected to promote the mixing of the oxidizer with the hot co-flow gas, and so the disturbance originating from the vortices possibly influenced the evolution of the main jet.

In the present study, we employed a constant co-flow gas mass flow rate regardless of temperature, and so the bulk velocity of the co-flow gas at T_C = 640 K was increased to 0.43 m/s. Brown et al. [8] reported increases in liftoff height along with the co-flow velocity. Min and Baillot [23] also found that data obtained with a co-flow velocity of 0.4 m/s were situated above Kalghatgi's correlation line, and concluded that this was due to confinement of the jet resulting from the higher co-flow velocity [44]. However, as shown in Figs. 6 and 7, the liftoff heights at T_C = 640 K were lower than those at T_C = 300 K, and the correlation at T_C = 640 K was situated below that obtained for T_C = 300 K. Moreover, as shown in Table 3, the value of C_1 at 640 K was comparable to that at 300 K. These trends appear to contradict those reported on the basis of previous studies [8][23], indicating the weak effect of increasing the co-flow velocity. It is evident that the effect of the co-flow velocity should be discussed in relation to the laminar burning velocity, since the liftoff height varies according to the

balance between the gas velocity and the burning velocity. In Min and Baillot's work [23], a co-flow velocity above 0.4 m/s was found to affect the liftoff height, which was comparable to the laminar burning velocity for pure methane. In contrast, the laminar burning velocity used in our model was increased to 0.81 m/s, and so was significantly higher than the co-flow velocity of 0.43 m/s. Based on consideration of the burning velocity, the effect of increasing the co-flow velocity on the liftoff height would be expected to be minimal.

As shown in Fig. 9, the DP2 model provided an excellent correlation even with hot co-flow gas. However, the correlation at T_C = 640 K exhibited a slight non-linearity, which is emphasized in Fig. 8(b). Previous studies [23, 26] reported similar results in which data for highly diluted flames deviated from Kalghatgi's line. However, in the present study, this trend was observed even in the case of undiluted flames (see the red circles plotted in Fig. 8(b)), indicating that this departure from linearity had a cause other than the high extent of dilution. Most likely, it can be attributed to the much lower liftoff height evident in Fig. 6. Almost all liftoff heights observed at T_C = 640 K were less than 40 mm (= 20 d_F), and Lawn [28] recommended that the premixed model be applied to flames lifted over 20 d_F. Joedicke et al. [13] demonstrated that a corrugated premixed flame appeared at the flame base at H = 30 d_F, while a triple flame was observed at H = 10 d_F. Because the premixed model is based on the formation of a turbulent premixed flame at the base, Joedicke's results reinforce Lawn's recommendation. Over the range of liftoff heights observed at T_C = 640 K, the flames were possibly in the process of transitioning to a state to which the premixed model can be applied. As a consequence, the slope of the correlation line varied with the liftoff height. The modeling of liftoff height throughout both the near and far fields will be a subject of future work by our group.

Finally, it is important to discuss the applicability of our model to other burner configurations, because the burner used in the present study was simpler than those employed

in conventional combustion furnaces. In the case that the velocity distribution within the combustion field is similar to that of a single jet, the model described herein can be applied. However, even for this simple type of burner, the value of C_1 in Eq. (2), which is a key parameter with regard to evaluating the degree of dilution caused by entrained gas, has been reported to vary widely [28]. Moreover, the evolution of the fuel jet is suppressed when the flame is confined either by a wall [45] or a high-speed co-flow [44]. Therefore, use of the present model presupposes a good understanding of the characteristics of the jet issued by the particular burner being assessed, in order to obtain a suitable C_1 value. In addition, if the turbulence intensity at the fuel inlet is varied, both the C_1 value and the position of the virtual origin must be adjusted on the basis of results obtained from experimental measurements. Otherwise, the model can either under- or over-predict the mass flow rate of entrained gas. It should also be noted that the introduction of a bluff body or swirl flow, which are commonly used to stabilize flames, will generate recirculation vortices in the reactant stream. These vortices will change the flow pattern of the fuel gas from a single jet to a stagnation flow [46], meaning that our model will be inapplicable to flames in which recirculation flow is present.

As shown in Table 1, the lowest concentration of oxygen in the co-flow gas was higher than the values observed in conventional furnaces, and so only a narrow range of oxygen concentrations was examined during the experimental trials. Further decreases in the oxygen concentration induced the blow-off of the lifted flame. Avoiding this effect will require increasing the co-flow gas temperature to compensate for the decreased burning velocity. Eventually, the lifted flame structure will transition to moderate or intense low-oxygen dilution (MILD) combustion, equivalent to an ignited flame [47]. Our model is based on a mechanism in which the gas and burning velocities are balanced, and can be applied to flames as long as this mechanism is maintained. Following a transition to MILD combustion,

the present model is therefore inapplicable, although the strategy used to evaluate the extent of dilution can be used to predict the ignition delay time.

6. Summary

The present study developed a premixed model capable of predicting the liftoff heights of turbulent non-premixed flames in combustion furnaces. In this model, the height is increased along with the extent of dilution resulting from the entrainment of burned gas but decreased by the temperature rise accompanying the dilution. The conditions in an actual combustion furnace were simulated in experimental trials using a triple concentric burner issuing fuel gas, oxidizer and high-temperature co-flow gas that mimicked the burned gas in a furnace. The conventional Kalghatgi premixed model, our previous DP1 model and our revised DP2 model were all assessed. The DP1 model included only the effects of decreasing reactant concentrations due to the entrainment of the co-flow gas (having a low O_2 concentration) whereas the DP2 model also included the effects of temperature increases.

The characteristics of non-reactive jets equivalent to fuel gas jets were initially investigated to obtain the parameters required to estimate the mass flow rate of the entrained co-flow gas, and liftoff heights were obtained from images of lifted flames. Decreases in the O_2 concentration in the co-flow gas were found to increase the liftoff height, while the associated temperature rise decreased the height.

The conventional premixed model failed to reproduce the unique correlation between the bulk velocities and liftoff heights of flames at a variety of O_2 concentrations and temperatures in the co-flow gas. The results obtained from the DP1 model demonstrated some improvement, in that data points for varying O_2 concentrations in the co-flow gas were located on a single line. However, the data for high-temperature co-flow gas separated from those acquired under room temperature conditions. The use of the DP2 model reduced this

separation effect by taking into account the increased laminar burning velocity resulting from the temperature increase. Introducing the effect of the virtual origin into the DP2 model provided a linear correlation of the liftoff height values at different O_2 concentrations and temperatures.

Although the DP2 model can exactly predict the liftoff heights of diluted flames, such predictions require detailed information regarding the characteristics of the fuel gas jet, including the spread rate, decay rate and virtual origin of the jet. Therefore, these data should be acquired prior to application of the model. In addition, the recirculation vortices that commonly appear above a bluff body or swirl burner can cause the flow pattern to deviate from the single jet scenario assumed in the present study. Hence, this model is currently inapplicable to flames above these types of burners. In the future, our group will attempt modeling of the liftoff heights of flames affected by recirculation.

Funding

This work was supported by the Japan Society for the Promotion of Science (JSPS) through a Grant-in-Aid for Scientific Research (C) (number 26420146).

References

[1] Fujimori T, Hamano Y, Sato J. Radiative heat loss and NOx emission of turbulent jet flames in preheated air up to 1230 K. Proceedings of Combustion Institute 2000; 28(1): 455-461. https://doi.org/10.1016/S0082-0784(00)80243-X

[2] Takahashi F, Schmoll WJ. Lifting criteria of jet diffusion flames. Symposium (International) on Combustion 1991; 23(1): 677-683. https://doi.org/10.1016/S0082-0784(06)80316-4

[3] Marin M, Baillot F. Experimental study of the lifting characteristics of the leading-edge of an attached non-premixed jet-flame: Air-side or fuel-side dilution. Combustion and Flame 2016; 171: 264-280. https://doi.org/10.1016/j.combustflame.2016.05.025

[4] Joedicke A, Peters N, Mansour M. The stabilization mechanism and structure of turbulent hydrocarbon lifted flames. Proceedings of Combustion Institute 2005; 30(1): 901-909. https://doi.org/10.1016/j.proci.2004.08.031

[5] Han D, Mungal MG. Observations on the transition from flame liftoff to flame blowout. Proceedings of Combustion Institute 2000; 28(1): 537-543. https://doi.org/10.1016/S0082-0784(00)80253-2

[6] Guiberti TF, Boyette WR, Krishna Y, Roberts WL, Masri AR, Magnotti G. Assessment of the stabilization mechanisms of turbulent lifted jet flames at elevated pressure using combined 2-D diagnostics. Combustion and Flame 2020; 214: 323-335. https://doi.org/10.1016/j.combustflame.2020.01.001

[7] Oh J, Khan QS, Yoon Y. Nitrogen dilution effect on flame stability in a lifted non-premixed turbulent hydrogen jet with coaxial air. Fuel 2010; 89(7): 1492-1498. https://doi.org/10.1016/j.fuel.2009.10.001

[8] Brown CD, Watson KA, Lyons KM. Studies on lifted jet flames in coflow: the stabilization mechanism in the near- and far-fields. Flow, Turbulence and Combustion 1999; 62: 249–273. https://doi.org/10.1023/A:1009925500084

[9] Hartl S, Van Winkle R, Geyer D, Dreizler A, Magnotti G, Hasse C, Barlow RS. Assessing the relative importance of flame regimes in Raman/Rayleigh line measurements of turbulent lifted flames. Proceedings of Combustion Institute 2019; 37(2): 2297-2305. https://doi.org/10.1016/j.proci.2018.06.067

[10] Watson KA, Lyons KM, Donbar JM, Carter CD. Simultaneous Rayleigh imaging and CH-PLIF measurements in a lifted jet diffusion flame. Combustion and Flame 2000; 123 (1-2): 252-265. https://doi.org/10.1016/S0010-2180(00)00133-4

[11] Muñiz L, Mungal MG. Instantaneous flame-stabilization velocities in lifted-jet diffusion flames. Combustion and Flame 2000; 111 (1-2): 16-30. https://doi.org/10.1016/S0010-2180(97)00096-5

[12] Oldenhof E, Tummers MJ, van Veen EH, Roekaerts DJEM. Ignition kernel formation and lift-off behaviour of jet-in-hot-coflow flames. Combustion and Flame 2010; 157: 1167-1178. https://doi.org/10.1016/j.combustflame.2010.01.002

[13] Choi BC, Kim KN, Chung SH. Autoignited laminar lifted flames of propane in coflow jets with tribrachial edge and mild combustion. Combustion and Flame 2009; 156(2): 396-404. https://doi.org/10.1016/j.combustflame.2008.10.020

[14] Li S, Qian W, Liu H, Liu G, Zhu M. Autoignition and flame lift-off behavior of a fuel jet mixing with turbulent hot air coflow. Proceedings of Combustion Institute 2020; in press. https://doi.org/10.1016/j.proci.2020.06.230

[15] Peters N, Williams FA. Lifftoff characteristics of turbulent jet diffusion flames. AIAA journal 1983; 21(3): 423-429. https://doi.org/10.2514/3.8089

[16] Vanquickenborne L, van Tiggelen A. The stabilization mechanism of lifted diffusion flames. Combustion and Flame 1966; 10(1): 59-69. https://doi.org/10.1016/0010-2180(66)90028-9

[17] Kalghatgi GT. Lift-off heights and visible lengths of vertical turbulent jet diffusion flames in still air. Combustion Science and Technology 1984; 41: 17-29. https://doi.org/10.1080/00102208408923819

[18] Miake-Lye RC, Hammer JA. Lifted turbulent jet flames: A stability criterion based on the jet large-scale structure. Symposium (International) on Combustion 1989; 22: 817-824. https://doi.org/10.1016/S0082-0784(89)80091-8

[19] Upatnieks A, Driscoll JF, Rasmussen CC, Ceccio SL. Liftoff of turbulent jet flames—assessment of edge flame and other concepts using cinema-PIV. Combustion and Flame 2004; 138(3): 259-272. https://doi.org/10.1016/j.combustflame.2004.04.011

[20] Ruetsch GR, Vervisch L, Liñán A. Effects of heat release on triple flames. Physics of Fluids 1995; 7(6): 1447-1454. https://doi.org/10.1063/1.868531

[21] Kim KN, Won SH, Chung SH. Characteristics of turbulent lifted flames in coflow jets with initial temperature variation. Proceedings of Combustion Institute 2007; 31(1): 1591-1598. https://doi.org/10.1016/j.proci.2006.07.236

[22] Wu Y, Al-Rahbi IS, Lu Y, Kalghatgi GT. The stability of turbulent hydrogen jet flames with carbon dioxide and propane addition. Fuel 2007; 86 (12-13): 1840-1848. https://doi.org/10.1016/j.fuel.2006.11.032

[23] Min J, Baillot F. Experimental investigation of the flame extinction processes of nonpremixed methane flames inside an air coflow diluted with CO2, N2, or Ar. Combustion and Flame 2012; 159 (12): 3502-3517. https://doi.org/10.1016/j.combustflame.2012.05.015

[24] Wang Q, Hu L, Zhang M, Tang F, Zhang X, Lu S. Lift-off of jet diffusion flame in sub-atmospheric pressures: An experimental investigation and interpretation based on laminar flame speed. Combustion and Flame 2014; 161 (4): 1125-1130. https://doi.org/10.1016/j.combustflame.2013.10.021

[25] Wilson DA, Lyons KM. Effects of dilution and co-flow on the stability of lifted non-premixed biogas-like flames. Fuel 2008; 87 (3): 405-413. https://doi.org/10.1016/j.fuel.2007.05.012

[26] Nada Y, Matsumoto K, Noda S. Liftoff heights of turbulent non-premixed flames in co-flows diluted by CO2/N2. Combustion and Flame 2014; 161 (11): 2890-2903. https://doi.org/10.1016/j.combustflame.2014.05.007

[27] Schlichting H. Boundary layer theory, sixth edition. 1968. McGraw-Hill, New York.

[28] Lawn CJ. Lifted flames on fuel jets in co-flowing air. Progress in Energy and Combustion Science 2009; 35(1): 1-30. https://doi.org/10.1016/j.pecs.2008.06.003

[29] Amielh M, Djeridane T, Anselmet F, Fulachier L. Velocity near-field of variable density turbulent jets. International Journal of Heat and Mass Transfer 1996; 39(10): 2149-2164. https://doi.org/10.1016/0017-9310(95)00294-4

[30] Lock A, Briones AM, Aggarwal SK, Puri IK, Hegde U. Liftoff and extinction characteristics of fuel- and air-stream-diluted methane–air flames. Combustion and Flame 2007; 149 (4): 340-352. https://doi.org/10.1016/j.combustflame.2007.02.007

[31] Kee RJ, Grcar JF, Smooke MD, Miller JA, Meeks E. PREMIX: A Fortran Program for Modeling Steady Laminar One-Dimensional Premixed Flame. Report No. SAND85-8240, Sandia National Laboratories 1985.

[32] Qin Z, Lissianski V, Yang H, Gardiner WC, Jr. Davis SG, Wang H. Combustion chemistry of propane: A case study of detailed reaction mechanism optimization. Proceedings of Combustion Institute 2000; 28: 1663-1669. https://doi.org/10.1016/S0082-0784(00)80565-2

[33] Zhao Z, Kazakov A, Li J, Dryer FL. The initial temperature and N2 dilution effect on the laminar flame speed of propane/air. Combustion Science and Technology 2010; 176: 1705-1723. https://doi.org/10.1080/00102200490487553

[34] Tang C, Huang Z, He J, Jin C, Wang X, Miao H. Effects of N2 Dilution on Laminar Burning Characteristics of Propane-Air Premixed Flames. Energy fuels 2009; 23(1): 151–156. https://doi.org/10.1021/ef800572v

[35] Liu F, Guo H, Smallwood GJ, Gülder ÖL. The chemical effects of carbon dioxide as an additive in an ethylene diffusion flame: implications for soot and NOx formation. Combustion and Flame 2001; 125 (1-2): 778-787. https://doi.org/10.1016/S0010-2180(00)00241-8

[36] Mi J, Nobes DS, Nathan GJ. Influence of jet exit conditions on the passive scalar field of an axisymmetric free jet. Journal of Fluid Mechanics 2001; 432: 91-125. https://doi.org/10.1017/S0022112000003384

[37] Pitts WM. Effects of global density ratio on the centreline mixing behavior of axisymmetric turbulent jets. Experiments in Fluids 1991; 11: 125-34. https://doi.org/10.1007/BF00190288

[38] Pitts WM, Kashiwagi T. The application of laser-induced Rayleigh light scattering to the study of turbulent mixing. Journal of Fluid Mechanics 1984; 141: 391-420. https://doi.org/10.1017/S0022112084000902

[39] Dowling DR, Dimotakis PE. Similarity of the concentration field of gas-phase turbulent jets. Journal of Fluid Mechanics 1990; 218: 109-41. https://doi.org/10.1017/S0022112090000945

[40] Uddin M, Pollard A. Self-similarity of coflowing jets: The virtual origin. Physics of Fluids 2007; 19: 068103. https://doi.org/10.1063/1.2740709

[41] Van KH, Oh S, Cha MS, Yoo CS, Park J, Chung SH. Effects of Schmidt number on non-monotonic liftoff height behavior in laminar coflow-jet flames with diluted methane and ethylene. Proceedings of the Combustion Institute 2021; 38: 1913-1921. https://doi.org/10.1016/j.proci.2020.06.344

[42] Van K, Jung KS, Yoo CS, Oh S, Lee BJ, Cha MS, Park J, Chung SH. Decreasing liftoff height behavior in diluted laminar lifted methane jet flames. Proceedings of the Combustion Institute 2019; 37: 2005-2012. https://doi.org/10.1016/j.proci.2018.05.031

[43] Van KH, Park J, Yoon SH, Chung SH, Cha MK. Mechanism on oscillating lifted flames in nonpremixed laminar coflow jets. Proceedings of the Combustion Institute 2019; 37: 1997-2004. https://doi.org/10.1016/j.proci.2018.07.052

[44] Wyzgolik A, Baillot F. Response of the non-premixed lifted flame to coaxial jet mixing layers. Proceedings of Combustion Institute 2007; 31(1): 1583-1590. https://doi.org/10.1016/j.proci.2006.07.214

[45] Noda S, Inohae J, Saldi ZS. NOx emission characteristics of confined jet nonpremixed flames. Proceedings of the Combustion Institute 2007; 31: 1625-1632. https://doi.org/10.1016/j.proci.2006.07.088

[46] Kalt PAM, Al-Abdell YM, Masri AR, Barlow RS. Swirling turbulent non-premixed flames of methane: Flow field and compositional structure. Proceedings of the Combustion Institute 2002; 29: 1913-1919. https://doi.org/10.1016/S1540-7489(02)80232-2

[47] Doan NAK, Bansude S, Osawa K, Minamoto Y, Lu T, Chen JH, Swaminathan N. Identification of combustion mode under MILD conditions using Chemical Explosive Mode Analysis. Proceedings of the Combustion Institute 2021; 38: 5415-5422

Table 1 Compositions (vol%) of fuel gas and co-flow gas during the combustion trials.

	Fuel gas			Co-flow gas		
	C_3H_8	N_2	CO_2	O_2	N_2	CO_2
LF1	70	30	0	21	79	0
	70	30	0	20	80	0
	70	30	0	19	81	0
	70	30	0	18	82	0
LF2	70	0	30	21	79	0
	70	0	30	20	75.2	4.8
	70	0	30	19	71.5	9.5

Table 2 Compositions (vol%) of fuel gas, oxidizer and co-flow gas during the concentration measurements.

	Fuel gas	Oxidizer	Co-flow gas
CO_2	68.3	5.3	0
O_2	6.7	0	21.0
N_2	25.0	94.7	79.0

Table 3 Jet parameters obtained from the concentration measurements.

T_C (K)	α_C	β_C	C_1	Virtual origin (mm)
300	9.1	78.9	138.8	-2.8
640	9.0	80.4	143.2	-9.0

1

Figure Captions

Figure 1 A diagram of the flow field near the base of a lifted flame.

Figure 2 Diagrams showing (a) a side view of the experimental apparatus and (b) a cross sectional view of the triple concentric burner.

Figure 3 Radial profiles of temperature at different heights beginning from the nozzle exit under non-reactive conditions.

Figure 4 Radial profiles of fuel mixture fractions in similarity form at different heights and at (a) T_C = 300 and (b) T_C = 640 K.

Figure 5 Evolution of the fuel gas jets as indicated by the (a) inverse of the fuel mixture fraction along the jet axis and (b) half-widths of jets determined from fuel mixture fractions.

Figure 6 Variation in the liftoff height with respect to the bulk velocity of the fuel gas under various conditions.

Figure 7 Liftoff height correlations based on (a) the conventional premixed model and (b) the DP1 model proposed in our previous study [26].

Figure 8 Liftoff height correlations obtained from the DP2 model for (a) n = 1.5 and (b) n = 1.0.

Figure 9 Liftoff height correlations obtained from the DP2 model combined with variations in the position of the virtual origin.

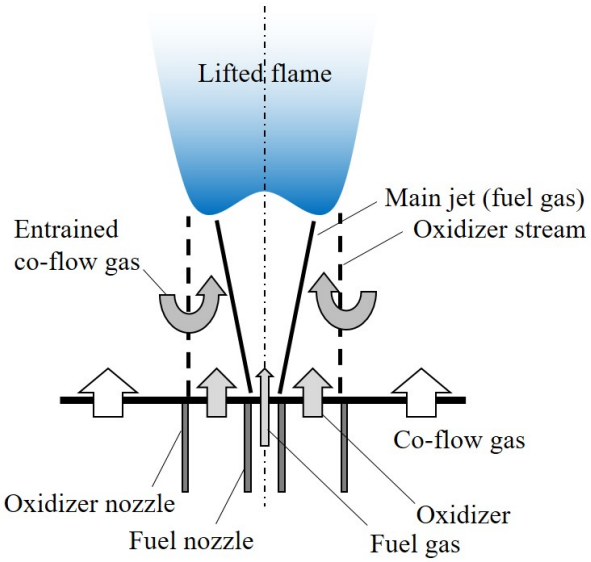

Fig. 1 A diagram of the flow field near the base of a lifted flame.

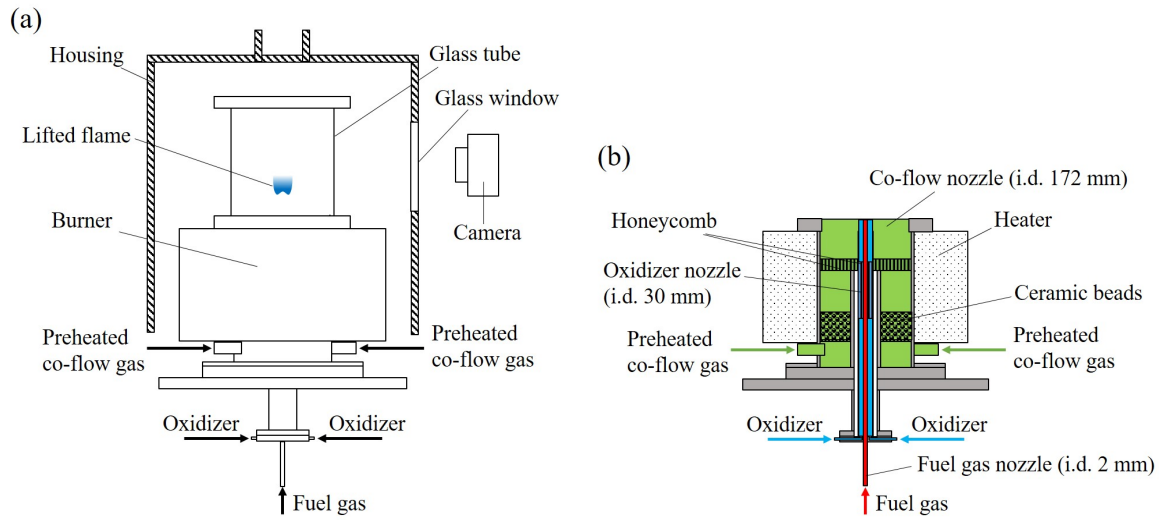

Fig. 2 Diagrams showing (a) a side view of the experimental apparatus and (b) a cross sectional view of the triple concentric burner.

1

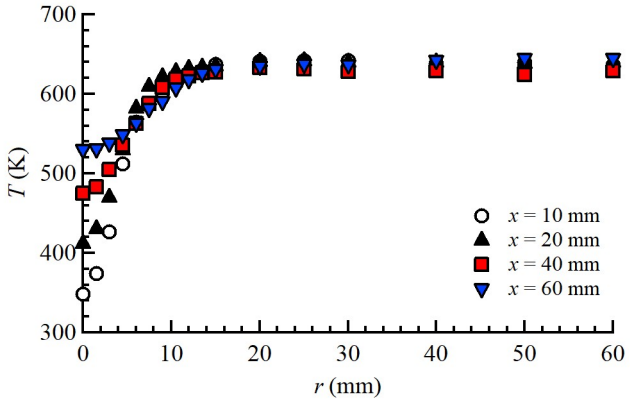

1

Fig. 3 Radial profiles of temperature at different heights beginning from the nozzle exit under non-reactive conditions.

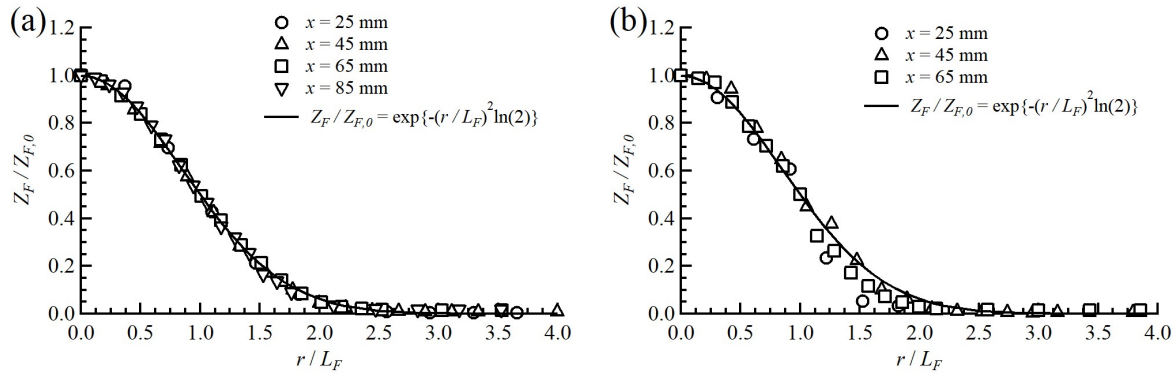

2

Fig. 4 Radial profiles of fuel mixture fractions in similarity form at different heights and at (a) T_C = 300 and (b) T_C = 640 K.

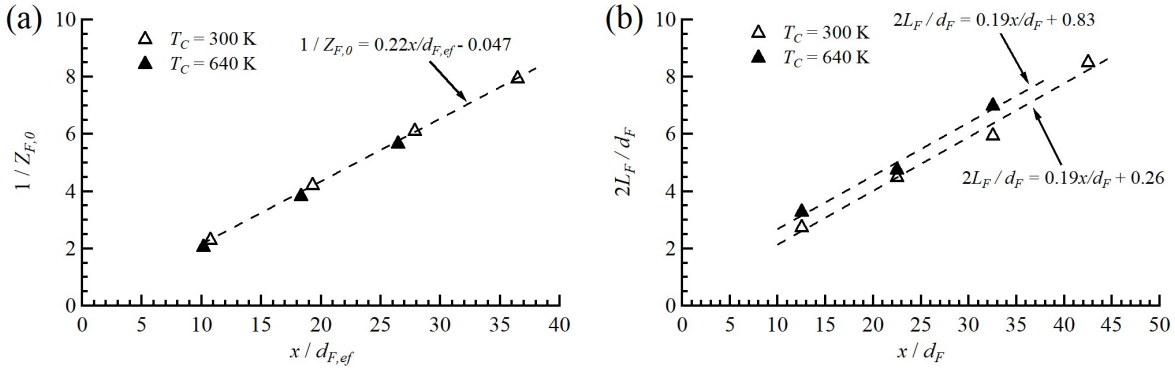

Fig. 5 Evolution of the fuel gas jets as indicated by the (a) inverse of the fuel mixture fraction along the jet axis and (b) half-widths of jets determined from fuel mixture fractions.

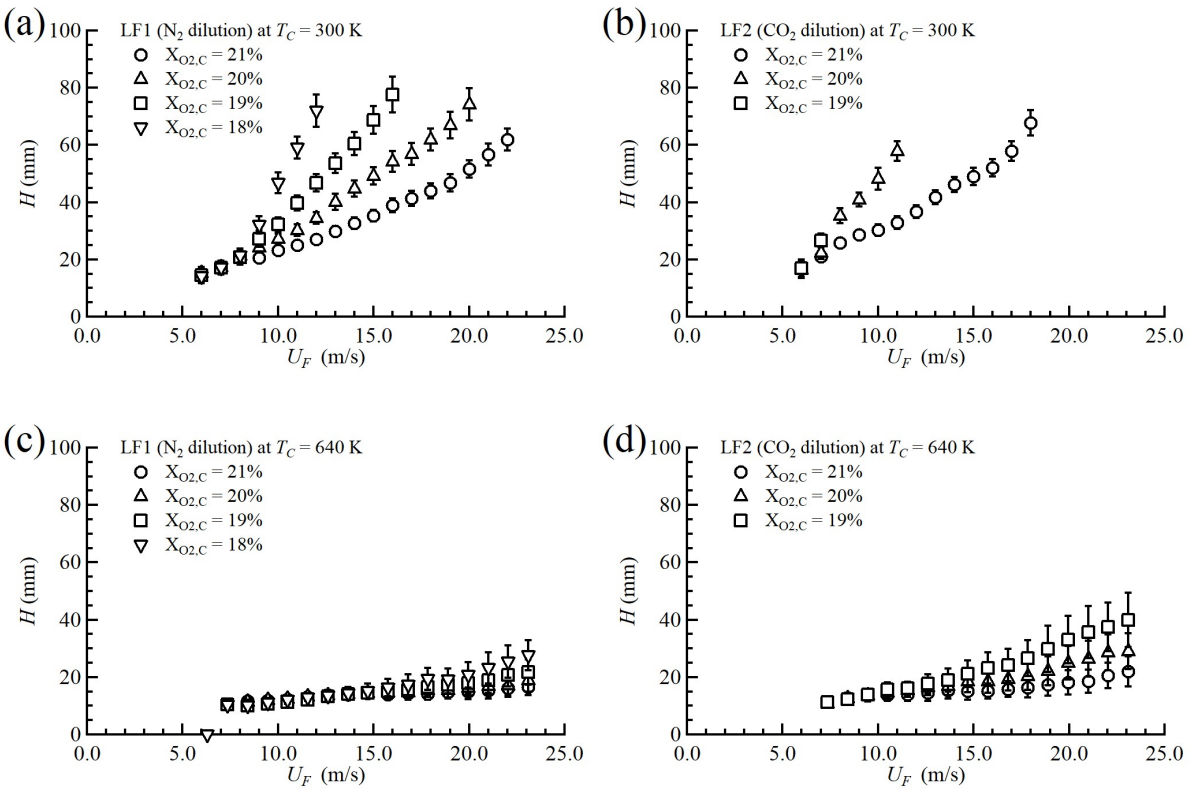

Fig. 6 Variation in the liftoff height with respect to the bulk velocity of the fuel gas under various conditions.

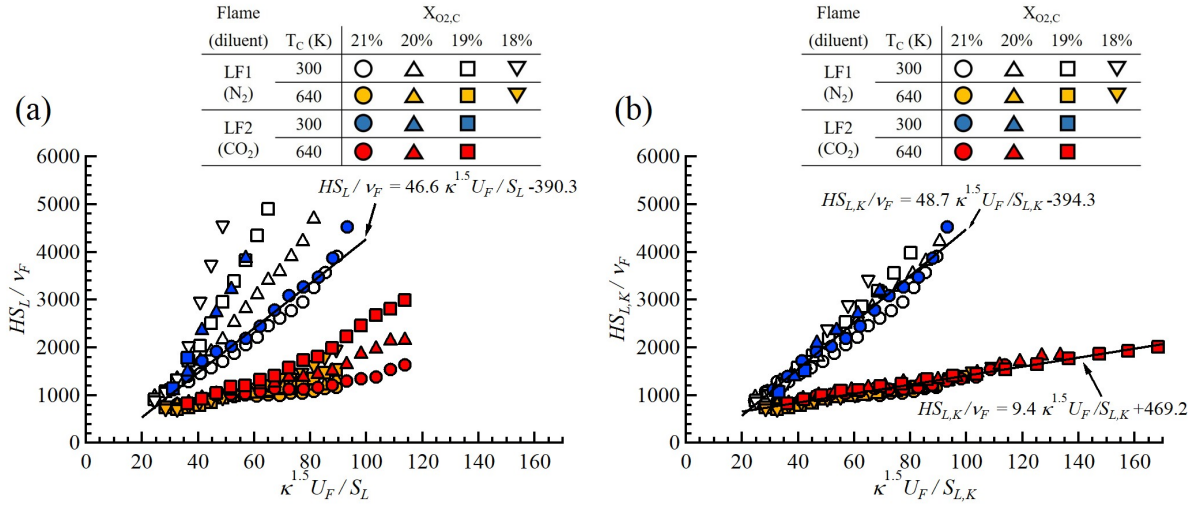

Fig. 7 Liftoff height correlations based on (a) the conventional premixed model and (b) the DP1 model proposed in our previous study [26].

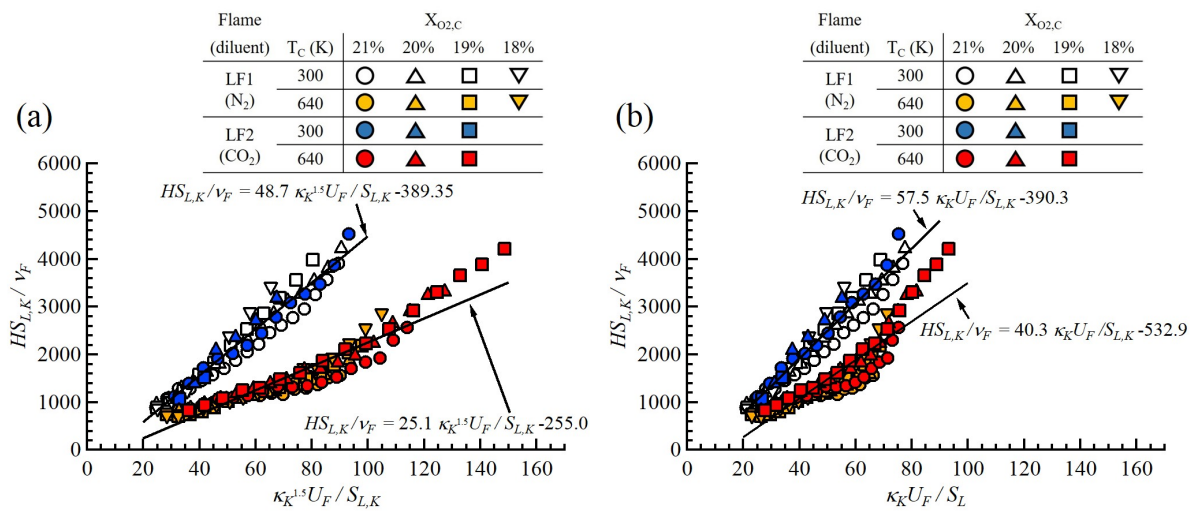

Fig. 8 Liftoff height correlations obtained from the DP2 model for (a) n = 1.5 and (b) n = 1.0.

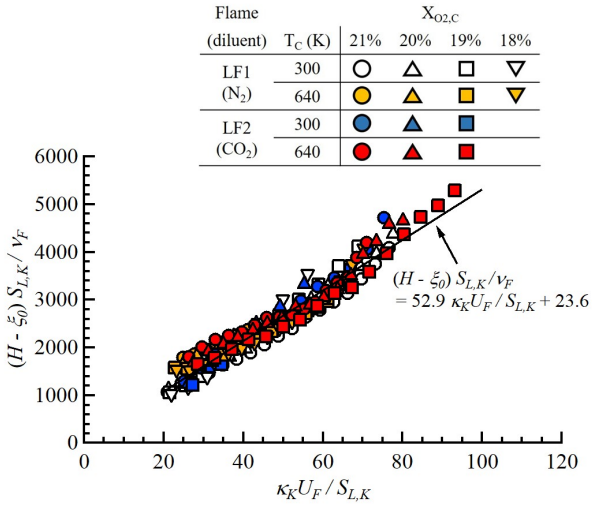

Fig. 9 Liftoff height correlations obtained from the DP2 model combined with variations in the position of the virtual origin.

1